Elaboration of lead-free Na0.5Bi0.5TiO3–BaTiO3 (NBT-BT) thick films by aerosol deposition method (ADM)

Marllory Isaza-Ruiz, Joseph Henon, Olivier Durand-Panteix, Gregory Etchegoyen, Fabrice Rossignol, Pascal Marchet

Elaboration of lead-free $Na_{0.5}Bi_{0.5}TiO_3$ – $BaTiO_3$ (NBT-BT) thick films by aerosol deposition method (ADM)

Marllory Isaza-Ruiz [a], Joseph Henon [a], Olivier Durand-Panteix [b], Gregory Etchegoyen [b], Fabrice Rossignol [c], Pascal Marchet [a, *]

a Université de Limoges, SPCTS, UMR 7315, F-87000 LIMOGES
b Centre de Transfert de Technologies Céramiques (CTTC), 7 rue Soyouz, Parc d'Ester, F-87068 LIMOGES
c CNRS, SPCTS, UMR 7315, F-87000 LIMOGES

* Corresponding author: Tel.: +33 5 87 50 23 73; fax: +33 5 87 50 23 04,
E-mail address: pascal.marchet@unilim.fr

Abstract
Thick and dense ceramic films of lead-free $0.94\ Na_{0.5}Bi_{0.5}TiO_3 - 0.06\ BaTiO_3$ (NBT-BT) composition were elaborated by aerosol deposition method (ADM) at room temperature. A powder of suitable grain size was elaborated by solid state reaction. Using this powder, two samples were elaborated by ADM respectively on glass and metallic substrates, in order to check for microstructure and electrical properties. This process allowed obtaining a thick film (3.2 μm) with dense microstructure. Measurement of electrical properties revealed a lossy dielectric behavior indicating interfacial phenomena at the electrode – film interface. The measurement of the ferroelectric hysteresis cycle does not show any characteristics of a ferroelectric behavior, but corresponds well to the one of a lossy non-linear dielectric. The absence of ferroelectricity is probably due to the low grain size of the obtained thick film (130 nm). Further experiments are in progress in order to try to obtain ferroelectric properties.

Keywords
Films, Dielectric properties, Functional applications, Lead-free perovskite materials, Aerosol Deposition Method,

1. Introduction
Piezoelectric materials have been in commercial use for about 50 years, and their utilization is still expanding. Nowadays, these materials are integrated in a wide range of devices using (i) direct piezoelectric effect, such as gas lighters, airbag sensors or more recently energy harvesting devices, (ii) converse piezoelectric effect such as position actuators, piezoelectric motors for cameras, piezoelectric injectors for motor cars, Micro Electromechanical Systems (MEMS) and (iii) both direct and converse effects, such as ultrasonic transducers for non-destructive testing, underwater sonar systems or medical imaging, parking sensors...

At the present time, most piezoelectric devices use PZT-based ceramic materials, *i.e.* a solid solution of general composition $PbZr_{(1-x)}Ti_xO_3$. Indeed, PZT are low cost compounds, easy to synthetize and to sinter, and they exhibit high electromechanical properties that make them highly suitable for a large range of applications. Unfortunately, PZT materials contain lead, thus their elaboration and use are associated to health and environmental issues. From 2006, the European Union adopted two directives concerning waste electrical and electronic equipments (WEEE) and restriction of the use of certain hazardous substances in electrical and electronic equipments (RoHS) [1, 2]. In December 2012, the European Chemicals Agency (ECHA) registered PZT in the candidate list of the REACH directive. Therefore, tremendous investigation efforts have been devoted to the development of lead-free materials presenting suitable properties for the replacement of PZT.

At the present time, the most promising candidates to the substitution of PZT are lead-free compounds of perovskite structure ABO_3. These materials are (i) alkali-niobates $(K,Na)NbO_3$ (KNN), (ii) barium titanate $BaTiO_3$ (BT) or barium titanates based compounds such as $(Ba,Ca)(Ti,Zr)O_3$ (BCTZ) and (iii) alkaline-bismuth titanates such as $Na_{0.5}Bi_{0.5}TiO_3$ (NBT) and $K_{0.5}Bi_{0.5}TiO_3$ (KBT) or solid solutions based upon these compounds such as $Na_{0.5}Bi_{0.5}TiO_3 - BaTiO_3$ (NBT − BT) [3-5].

Furthermore, some of the abovementioned applications, such as piezoelectric sensors, energy harvesting systems, position actuators or MEMS require elaboration as thick films for the active piezoelectric material. In the past, ceramic thick films were realized by different methods such as CVD or PVD, plasma spraying, solid-state reaction, screen printing or tape casting. The main disadvantages of these methods are the requirement of (i) heating of the substrate during deposition or (ii) thermal post-treatment for sintering and/or crystallization. Thus this problem limits the use of such materials on substrates like metals or polymers.

Recently, a new deposition technic suitable for the elaboration of ceramic films at room temperature, the Aerosol Deposition Method (ADM), was developed by J. Akedo *et al.* [6]. A large panel of materials has already been deposited by ADM: metals and alloys [7-10], simple and complex ceramic oxides such as apatite [11], ferrites [12], perovskites [13-19], spinel [20]... More recently, ADM has been used for the elaboration of composite materials such as ceramic-ceramic [21,22] , ceramic-metal [23] , or ceramic-polymer combinations [24,25]. In this method, a powder is first mixed with a gas in order to produce a dry aerosol inside a chamber called "aerosol generator" (see fig. 2). This aerosol is then carried through a pipe, linking the aerosol generator and the deposition chamber, itself connected to a vacuum pump. The differential pressure between the two chambers allows the aerosol to be transferred up to a nozzle where it is accelerated. Thus, the particles impact the substrate at a very high velocity (150-500 $m.s^{-1}$) [26]. A part of the kinetic energy of particles is directly converted into bonding energy between the substrate and the particles and also between the particles themselves. Thus, the ceramic powder is directly consolidated as a dense layer. This phenomenon was consequently named "room temperature impact consolidation" [26]. As a counterpart, some disadvantages are observed: (i) reduction of crystallite size and (ii) deformation of deposited particles.

Thus ADM presents several interesting features compared to other deposition technics: (i) a large range of thickness can be obtained (0.5μm – 100μm), (ii) the deposition rate is quite high (up to 50 μm/min) [27] , (iii) thick films with the same composition and crystalline structure as those of the starting powder can be obtained even for complex materials [28], (iv) complex geometries can be obtained easily using a deposition mask [6, 13] and (v) finally, dense films are obtained at room temperature without further heat treatment of the deposited material [6]. Consequently, many kinds of substrates are allowed (including "fragile" substrates) like glass, metals and polymers [29].

Concerning piezoelectric materials, the ADM method has already been successfully used for the deposition of lead-based materials such as PZT and PZT–based compounds [13, 26, 30]. The corresponding studies also evidenced some important features of ADM process: (i) the morphology, size and aggregation state of the deposited powders are key parameters to obtain thick and dense films [30], (ii) due to the high impact velocity, the crystalline size of deposited ceramic material is drastically reduced compared to the starting powder, leading to sub-micronic ceramic grains in the thick film [13, 26]. The ferroelectric / piezoelectric properties are mainly determined by ferroelectric domains size and thus widely depend on grain size. As a consequence, a (short) post-deposition annealing (600°C – 5 min) was required in order to obtain suitable ferroelectric-piezoelectric properties [13, 30]. PZT-based piezoelectric devices were successfully elaborated by ADM after such a post-deposition annealing [31].

Concerning lead-free materials, only a few papers reported results on the elaboration of thick films by ADM. $BaTiO_3$ films were successfully obtained on Cu and stainless steel substrates [14, 32]. The influence of thickness on dielectric properties was studied and a critical thickness was evidenced (around 1μm), below which high leakage currents and low resistivity were observed because of the inhomogeneity of the interface between the film and the substrate. [33], but ferroelectric properties were not reported. For KNN, thick films were successfully obtained on Pt/Sapphire substrates [34]. As for PZT, the ferroelectric properties were obtained only after annealing at 700°C for 1h. NBT films were deposited on $Pt/Ti/Al_2O_3$ and sapphire substrates by the Akedo's group for which ferroelectric properties were again obtained only after annealing at 1000°C for 1h [35, 36].

But at the present time, there is no report on the elaboration of NBT-BT films by ADM. However, NBT-BT composition is considered as one of the possible materials for the substitution of lead-based piezoelectric materials [3-5]. Thus the aim of the present study is: (i) to obtain thick and dense ceramic films of $0.94\ Na_{0.5}Bi_{0.5}TiO_3 – 0.06\ BaTiO_3$ composition (NBT – BT) and (ii) to check their electrical properties in order to determine if ferroelectric properties can be achieved without post-annealing treatment.

2. Material and methods

A batch of powders of $0.94\ Na_{0.5}Bi_{0.5}TiO_3 – 0.06\ BaTiO_3$ composition (hereafter referenced as powder #1) was elaborated through solid state reaction, using Bi_2O_3 (Alfa-Aesar 99.9995%), Na_2CO_3 (Aldrich 99.5%), $BaCO_3$ (Alfa-Aesar 99.8%) and TiO_2 (Alfa-Aesar 99.8%). Stoichiometric amounts of the precursors were weighed and mixed in ethanol using

planetary milling with zirconia balls (250 rpm, 5 h). The mix was then dried and de-agglomerated using agate mortar, heat treated using the parameters reported in fig. 1 and finally milled again. In order to remove the coarse agglomerates, the obtained powder was sieved (40 μm sieve) and then stored in a dryer until use. This powder was characterized by X-ray diffraction (XRD, Bruker D8 advance, Cu Kα, 2θ range 10–70°, scanning step 0.013°), scanning electron microscopy (SEM, JEOL 7400) and laser granulometry (laser particle size analyzer HORIBA Partica LA-950). The lattice parameters were calculated by using a global refinement of the full diagram, with the "pattern matching" process of the Rietveld method (Jana 2006 software) [37].

With these powder (powder #1), thick films were deposited using an ADM device developed by the Center for Technology Transfers in Ceramics (CTTC) in collaboration with the SPCTS laboratory. Its description was detailed in previous work [29]. Particles were transported with nitrogen carrier gas at a flow rate of 7 L/min and accelerated through a nozzle with a rectangular orifice size of 0.2 mm × 5 mm. The substrate was placed at a distance of 1.5 mm. The deposition time was 4 min and the deposition area was 5 mm × 12 mm (fig.2). The samples were elaborated at room temperature using a 1mm/s substrate displacement velocity and 10 scans back and forth during deposition. Two samples were realized: one using a thin metallic substrate and another one using a glass substrate (table 1). The metallic substrates used for this study are standard steel foils of 20 μm in thickness and standard borosilicate glass substrates. The sample #1a elaborated on glass substrates is devoted to most of the characterizations, while sample #1b on metallic substrates was only used for measurement of electrical properties. After deposition, the samples were characterized by XRD, SEM and atomic force microscopy (AFM). The thickness was determined only for sample #1a deposited on glass substrate, since for metallic substrates the hardness was too low to perform measurements. The thickness of sample #1a was measured using a mechanical profilometer (Dektak) and estimated to be identical for sample #1b elaborated on metallic substrates using the same deposition parameters. The surface roughness was determined for sample #1a using AFM, together with the mean grain size, determined by image analysis of AFM results. The electrical properties were determined between 100 Hz and 1 MHz using an impedance analyzer (Agilent 4294 A), for samples #1b deposited on metallic substrate. The metallic substrate himself was used as base electrode, while several top electrodes (platinum, 3 mm in diameter and 100 nm in thickness) were elaborated by DC-sputtering in order to obtain well-defined measurement areas. Finally, the ferroelectric hysteresis cycles was measured for the same configuration (sample 1b) using a ferroelectric tester devoted to films (Radiant).

3. Results and discussion
3.1 Characterizations of the powder:
The SEM pictures of powder #1 show a high agglomeration state, with constituting particles around 0.15 μm (fig. 3.a). Inside this agglomerates, the constituting elementary grains appears as linked by a "pre-sintering" process. Thus this grains are probably not only agglomerated by short range interactions, but chemically linked by bridges between the constituting particles.

Measurement of the particle size revealed two different populations in terms of volume fraction, one around 0.15 μm and the second one around 1 μm (fig. 3.b). The first population probably corresponds to the constituting elementary grains, while the last one is associated to the agglomerates as revealed by SEM pictures.

For this powder, X-ray diffraction evidenced for a perovskite compound, corresponding well to the JCPDS 12-546 file, reported for NBT-5.5% BT (fig. 4). According to the 0.94 $Na_{0.5}Bi_{0.5}TiO_3$ − 0.06 $BaTiO_3$ initial composition, the structure is rhomboedral with calculated lattice parameters (hexagonal axes) a = b = 5.498 ± 0.001 Å, c = 13.5085 ± 0.001 Å ($\alpha = \beta = 90°$, $\gamma = 120°$). The Scherrer formula gave an order of magnitude of 30-50 nm for the size of the diffracting crystallites .

3.2. Characterization of the thick film
3.2.1. Structure and microstructure

As said in the introduction, the purpose of this study was to obtain thick and dense ceramic films of 0.94 $Na_{0.5}Bi_{0.5}TiO_3$ − 0.06 $BaTiO_3$ composition (NBT − BT). X-ray diffraction pattern of sample #1a (glass substrate) was determined using the same parameters as for powder (fig. 4). Taking into account the low quantity of material irradiated by the incident X-ray beam, the observed intensities are lower than for powders, but the diffraction peaks are observed at the same 2θ angles. This indicates that the deposited material presents the same perovskite structure as the initial powders. Furthermore, the width of the diffraction peaks is much greater than for the initial powders. It can be inferred that the size of diffracting crystallites is much lower, and probably in the order of magnitude of 10 − 100 nm. Indeed, a rough estimation of the size of the diffracting crystallites, based upon the Scherrer formula, gave an order of magnitude of 10-15 nm. This indicates that the size of diffracting crystallites was slightly reduced during the ADM process.

The microstructure of the films was studied by SEM and AFM for sample #1a (fig. 5). The AFM pictures reveal homogeneous microstructure, presenting a lot of craters. The mean roughness (AFM scans) is around 100nm (table 2), i.e. the same order of magnitude as the constituting particles of the starting powder. SEM observations reveal craters, in which fragmented particles are observed (see insert of fig 5.c). The cross-section SEM view shows a dense lamellar stacking of grains (fig. 5.d), without porosity. This observation confirms that the grains are fragmented and flattened during ADM process, thus leading to a dense film.

The mean grain size determined by AFM is around 130 nm (table 2). This value is a little bit larger than the size of the particles constituting the agglomerates in the starting powder, and widely smaller than the size of the initial agglomerates. This means that due to high impact velocity, the morphology of the powder grains is dramatically modified, leading to their fragmentation. The cross section view (fig. 5.d) confirms that the grains are fragmented and flattened during ADM process, thus leading to a dense film. This observation agrees with the large decrease of grain size during ADM process reported in previous studies, due to high impact velocity of particles [13, 26]. This phenomenon was also confirmed by other experiments (not reported here) using a powder of larger grain size. In this case, the

mean grain size of the obtained film was of the same order of magnitude as for sample #1a. But the obtained film was thinner and porous, thus non-suitable for applications.

3.2.2. Electrical properties

As a first basic step, the impedance and phase angle were measured for sample #1b deposited on metallic substrates, confirming a dielectric behavior. Meaurement of the dielectric properties (fig. 6 a) revealed that the relative permittivity of this sample is around 230 at 100 Hz and decreases up to 90 at 1 MHz. The dielectric losses are high for low frequency (37% at 100 Hz), decrease up to 9-10% for 10 kHz and then increase quickly for higher frequency (up to 65% at 1 MHz). The high value of dielectric losses at low frequency probably indicates interfacial phenomena at the electrode − film interface. The high values of $\tan(\delta)$ at high frequency indicates the probable occurrence of charge carriers (like vacancies) inside the deposited material. This is not surprising since during the ADM process , the kinetic energy of the particules is very high and dissipated during a very short time, thus inducing crystalline defects. However, these observations mean that this sample has the behavior of a lossy dielectric.

The ferroelectric properties were also measured for sample #1b. The results confirm the dielectric characterization (fig. 6.b). Indeed, even if a cycle is observed, the shape of this cycle corresponds more to a lossy dielectric than to a true ferroelectric material [38]: (i) the saturation is not observed for high fields and on the contrary, the measured polarization decreases for high fields, probably because of a charge injection phenomenon (see red rectangles in fig.6.b), (ii) there is no "concave" region in P versus V curve (see blue arrows in fig. 6.b). The shape of the P versus V cycle suggests non-linear behavior, similar to the one observed for thin films of ferroelectric materials but presenting poor crystalline quality. As a consequence, the ferroelectric behavior is not confirmed for this sample. A first attempt to improve the ferroelectric properties by annealing at $0.94\ Na_{0.5}Bi_{0.5}TiO_3 − 0.06\ BaTiO_3$ increased slightly the dielectric losses but did not change the hysteresis cycle.

The sample #1b is thick (3.2 μm) and dense, but mean grain size determined by AFM (0.130 μm) is on the order of magnitude of 100 - 150 nm and does'nt present ferroelectricity. This corresponds well to the grain size effect observed for ferroelectric ceramics materials; For example, $BaTiO_3$ ceramics with grain size lower than around 100 nm are not ferroelectrics, because grain size is too small to allow for the occurrence of ferroelectric ordering and so the structure is no more tetragonal but becomes cubic [39-41]. This behavior also corresponds well to previous results obtained by ADM: ferroelectric behavior was only obtained after thermal annealing of the films [13, 30, 31, 34-36,].

Conclusion

The aim of this study was (i) to obtain thick and dense ceramic films of $0.94\ Na_{0.5}Bi_{0.5}TiO_3 − 0.06\ BaTiO_3$ composition (NBT –BT) and (ii) to check for their electrical properties in order to determine if ferroelectric properties can be achieved without post-annealing treatment. Thick films of NBT-6%BT were successfully obtained for the first time by ADM method using a powder elaborated by solid-state reaction at 850°C/4h. The thickness

of this film is around 3.2 μm, with a dense microstructure presenting some craters due to the impact of the powder during the deposition process. The resultant mean grain size is around 130nm, thus too low to present ferroelectricity. As a consequence, this film presents insulating behavior, with high dielectric losses. The measurement of the ferroelectric hysteresis cycle does not show any characteristics of a ferroelectric behavior, but corresponds well to the one of a lossy non-linear dielectric. The absence of ferroelectricity is probably due to the low grain size, since for ceramics small grain size destroys ferroelectricity. Further experiments are in progress in order to confirm this hypothesis by post-annealing to cause grain growth.

References

[1] Directive 2002/95/EC On the restriction of the use of certain hazardous substances in electrical and electronic equipment, Official Journal of the European Union, 13.2.2003, L37/19 – L37/23

[2] Directive 2002/96/EC On waste electrical and electronic equipment (WEEE), Official Journal of the European Union, 13.2.2003, L37/24 – L37/38

[3] J. Rodel, W. Jo, T.P. Seifert, E. M. Anton, T. Granzow, D. Damjanovic, perspective on the development of Lead-free Piezoceramics, J. Am. Ceram. Soc. 92 (2009) 1153-1177

[4] P. K. Panda, Review: environmental friendly lead-free piezoelectric materials, J. Mat. Sci. 44 (2009) 5049-5062

[5] J. Rodel, G. Webber Kyle, R. Dittmer, W. Jo, M Kimura, D. Damjanovic D, Transferring lead-free piezoelectric ceramics into applications, J. Eur. Ceram. Soc. 35 (2015) 1659-1681

[6] J. Akedo, Aerosol deposition (AD) integration techniques and their application to microdevices, In: M. Singh M, T. Ohji, R. Asthana, S. Mathur S, editors, Ceramic integration and joining technologies: from Macro to Nanoscale, EPUB E-Book, 2011, p. 489-520

[7] H.Y. Kim, J.W. Lee, H.J. Kim, S.M. Nam, Silver metallization for microwave device using aerosol deposition, Ceram. Int. 38 (2012) S201-4

[8] S. Baba, L. Uhang, H. Sato, R. Funahashi, J. Akedo, Room temperature fast deposition and characterization of nanocrystalline ($Bi_{0.4}Sb_{1.6}Te_3$) thick films by aerosol deposition. J. Phys Conf. Ser. 379 (2012) [article 01211, 1-7]

[9] S. Sugimoto, M. Nakamura, T. Maki, T. Kagonati, K. Inomata, J. Akedo & al. $Nd_2Fe_{14}B/Fe_3B$ nanocomposite film fabricated by aerosol deposition method. J. Alloys Compd. 408 (2006) 1413-1416

[10] S. Sugitomo, T. Hirayanma, T. Maki, T. Koganati, K. Inomata, J. Akedo, Fabrication of anisotropic SmFeN films using the aerosold deposition method, Jpn. Soc. Powder Metall. 53 (2006) 258-2262

[11] D.S. Park, I.S. Kim, H. Kim, A.H.K. Chou, B.D. Hahn, L.H. Li & al., Improved biocompatibility of hydroxyapatite thin film prepared by aerosol deposition, J. Biomed. Mater. Res.: Appl. Biomater. 94 (2010) 353-358

[12] M. Lebedev, J. Akedo, A. Iwata, S. Sugimoto, K. Inomata, NiZnCu ferrite thick film with nano scale crystallites formed by the aerosol deposition method, J. Am. Ceram. Soc. 87 (2004) 1621-1624

[13] J. Akedo, Room temperature impact consolidation (RTIC) of fine ceramics powder by aerosol deposition method and applications to microdevices, J. Therm. Spray Technol. 17 (2008) 181-198

[14] J.M. Oh, S.M. Nam, Role of surface hardness of substrate in growing $BaTiO_3$ thin films by aerosol deposition method, Jpn. J. Apll. Phys. 48 (2009) [article 09KA07, 1-5]

[15] J.J. Choi, J. Ryu, B.D. Hahn, W.D. Yoon, D.S. Park, Room temperature conducting $LaNiO_3$ thick film coatings prepared by aerosol deposition, J. Am. Ceram. Soc. (91) 2008 2756-2758

[16] Y.C. Wu, S.F. Wang, L.G. Teng, Microstructures and dielectric properties of $MgTiO_3$ thick film prepared using aerosl deposition method, Ferroelec. 435 (2012) 135-147

[17] J.J. Choi, J.H. Lee, D.S. Park, B.D. Hahn, W.H. Yoon, H.T. Lin, oxidation resistance coating of LSM and LSCF on SOFS metallic interconnects by the aerosol deposition process, J. Am. Ceram. Soc. 90 (2007) 1926-1929

[18] J.J. Choi, J.H. Choi, J. Ryu, B.D. Hahn, J.W. Kim, C.W. Ahn & al. Low temperature fabrication of nano-structured porous $(La,Sr)(Co,Fe)O_{3-\delta}$ cathodes by aerosol deposition, J. Alloys Compd. 545 (2012) 186-189

[19] J.H. Kim, Y.M. Kang, M.S. Byun, K.T. Hwang, Study on the chemical stability of Y-doped $BaCeO_{3-\delta}$ and $BaZrO_{3-\delta}$ films deposited by aerosol deposition, Thin Solid Films 520 (2011) 1015-1021

[20] J Ryu, K.Y. Kim, J.J. Choi, B.D. Hahn, W.H. Yoon, B.K. Lee & al. Highly dense and nanograined $NiMn_2O_5$ negative temperature coefficient thermistor thick film fabricated by aerosol-deposition, J. Am. Ceram. Soc. 92 (2009) 3984-3087

[21] M. Nakada, T. Kawakami, M. Iwanami, K. Ohashi, Application of electronics devices for aerosol deposition methods, Nec. Tech. J. 2 (2007) 76-80

[22] J. Ryu, J.J. Choi, B.D. Hahn, W.H. Yoon, B.K. Lee, H.H. Choi & al. $Pb(Zr, Ti)O_3 - Pb(Mn_{1/3}Nb_{2/3})O_3$ piezoelectric thick films by aerosol deposition, Mater. Sci. Eng. B 170 (2010) 67-70

[23] Y. Imanama, H. Amada, F. Humasaka, Microstructure and dielectric properties of composite films for embedded capacitor applications, Int. J. Appl. Ceram. Technol. 8 (2011) 653-675

[24] H.J. Kim, Y.H. Kim, S.M. Nam, Y.J. Yoon, J.H Kim, Calculations of Al_2O_3 contents in Al2O3-PTFE composite thick films fabricated by using the aerosol deposition, J. Korean Phys. Soc. 57 (2010) 1086-1091

[25] B.D. Hahn, D.S. Park, J.J. Choi, J. Ryu, W.H. Yoon, J.H. Choi & al. Aerosol deposition of hydroxyapatite-chitosan composite coatings on biodegradable magnesium alloy, Surf. Coat. Technol. 201 (2011) 2112-3118

[26] J. Akedo, Aerosol deposition of ceramic thick films at room temperature: densification mechanism of ceramic layers, J. Am. Ceram. Soc. 98 (2006) 1834-1839

[27] J. Akedo, M. Lebedev; A. Iwata, S. Nakano, H. Ogiso, Aerosol deposition for nanocomposite material synthesis - a novel method of ceramic processing without firing. Ceram. Eng. Sci. Proc. 24 (2003) 9-14

[28] J. Henon, M.A. Piechowiak, O. Durand-Panteix, G. Etchegoyen, O. Masson, C. Dublanche-Tixier, P. Marchet, B. Lucas, F. Rossignol, Dense and highly textured coatings obtained by aerosol deposition method from Ti_3SiC_2 powder: Comparison to a dense material sintered by Spark Plasma Sintering, J. Eur. Ceram. Soc. 35 (2015) 1179-1189

[29] M.A. Piechowiak, J.M. Henon, O. Durand-Panteix, G. Etchegoyen, V. Coudert, P. Marchet, F. Rossignol, Growth of dense Ti_3SiC_2 MAX phase films elaborated at room temperature by aerosol deposition method, J. Eur. Ceram. Soc. 34 (2014) 1063-1072

[30] Y. Kawakami, H. Yoshikawa, K. Komagata, J. Akedo, powder preparation for 0.5 Pb(Ni$_{1/3}$Nb$_{2/3}$)O$_3$ − 0.15 PbZrO$_3$ − 0.35PbTiO$_3$ thick films by the aerosol deposition method, J. Cryst. Growth 275 (2005) e1295-e1300

[31] J.H. Park, Y. Park, J. Akedo, Temperature properties of PZT actuated High-speed metal-based optical resonant scanners, in IEEE International Symposium on Applications of Ferroelectrics, IEEE editor, 2007, 711-713

[32] H. Hatano, T. Ito, K. Iwata, Multilayer construction with various ceramic films for electronic devices fabricated by aerosol deposition, Int. J. Appl. Ceram Tech. 3 (2006) 419-427

[33] J.M. Oh, N.H. Kim, S.C. Choi, S.M. Nam, thickness dependence of dielectric properties on BaTiO$_3$ films fabricated by aerosol deposition method, Mat. Sci. Eng. B 161 (2009) 80-84

[34] G. Han, C.W. Ahn, J. Ryu, W.H. Yonn, J.J. Choi, B.D. Hanh, J.W. Kim, J.H. Choi, D.S. Park, Effect of tetragonal perovskite phase addition on the electrical properties of KNN thick films fabricated by aerosol deposition, Mat. Lett. 65 (2001) 2762-2764

[35] M. Suzuki, Y. Noguchi, M Miyayama, J. Akedo, Polarization and leakage current properties of bismuth sodium titanate ceramic films deposited by aerosol deposition method, J. Ceram. Soc. Jpn. 118 (2010) 899-902

[36] M. Suzuki, J. Akedo, Polarization and leakage current properties of self-supported bismuth sodium titanate ceramic films deposited by aerosol deposition method, J. Ceram. Soc. Jpn. 121 (2013) 664-669

[37] V. Petricek, M. Dusek, L. Palatinus, Crystallographic Computing System JANA2006: General features, Z. Kristallogr. 229 (2014), 345-352.

[38] J.F. Scott, Ferroelectrics go bananas, J. Phys: Condens. Matter. 20 (2008) 021001

[39] K. Uchino, E. Sadanaga, T. Hirose, Dependence of the crystal structure on particle size in barium titanate, J. Am. Ceram. Soc. 72 (1989) 1555-1558

[40] Z. Zhao, V. Buscaglia, M. Viviani, M.TM Buscaglia, L. Mitoseriu, A. Testino, M. Nygren, M. Johnsson, P. Nanni, Grain-size effects on the ferroelectric behavior of dense nanocrystalline BaTiO$_3$ ceramics, Phys. Rev. B 70 (2004) 024107

[41] M. Tyunina, B. Malic, M. Plekhn M. Kosec, Dielectric response of BaTiO$_3$ thin film with grain size at nanometer scale, J. Am. Ceram. Soc. 95 (2012) 1333-1338

Powder	Thick film sample	substrate	Characterizations performed
#1	#1a	Glass	XRD, profilometer, SEM, AFM
	#1b	Metal (0.02 mm in thickness)	Impedance, hysteresis cycles

Table 1: correspondence between powder batch and ADM films

Sample	Thickness (µm) : profilometer	Roughness (µm) : AFM	Mean grain size (µm) : AFM
#1a	3.18	0.097	0.136

Table 2: thickness, roughness and mean grain size of the ADM thick films samples

Figure caption

Fig. 1: Bloc diagram corresponding to the synthesis of powder #1

Fig. 2: Scheme of the Aerosol Deposition Device (ADM)

Fig. 3: SEM Pictures and particle size distribution for the powder #1 (a & b) (magnification 2000, white bar = 10µm: insert magnification 30000).

Fig. 4: X-ray diffraction pattern of powder (top) and thick film (bottom); The Miller index corresponds to red lines on lower part of the figure (JCPDS 012--5546 pattern of NBT-5.5% BT)

Fig. 5: microstructure of sample 1 as determined by AFM for a 50µm X 50µm zone (a), 3-D picture of the same surface (b), SEM picture of the surface (magnification 10000, white bar = 1 µm; insert magnification 100000) and SEM picture of the vertical section of the sample (magnification 5000, white bar = 1 µm)

Fig 6: (a) relative permittivity and dielectric losses for sample 1b deposited on metallic substrate and (b) hysteresis cycle for the same sample (see text for blue arrows and red rectangles).
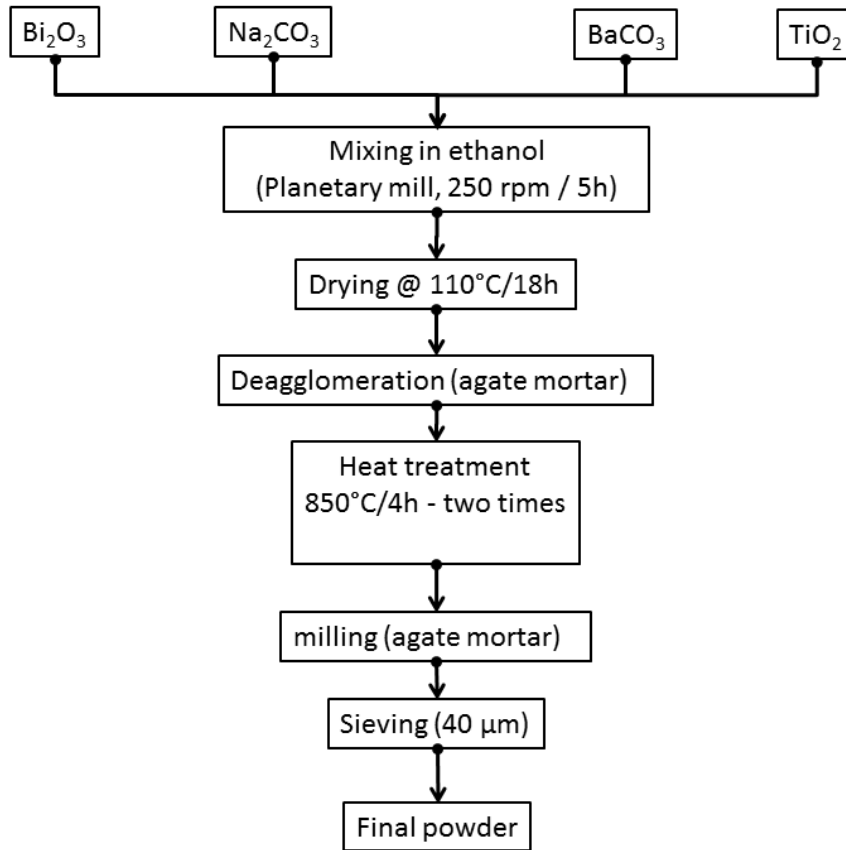
Fig. 1: Bloc diagram corresponding to the synthesis of powders #1.
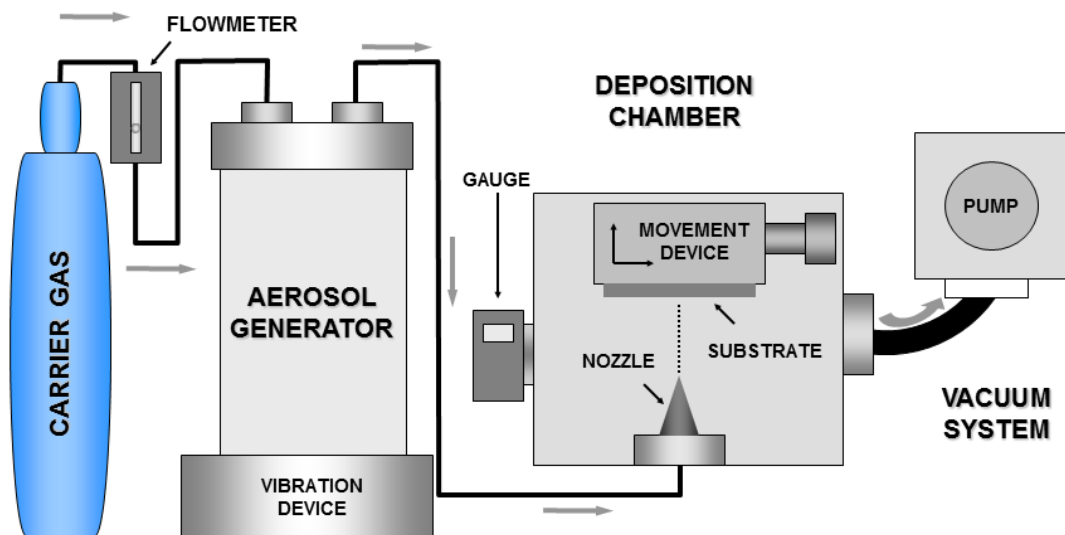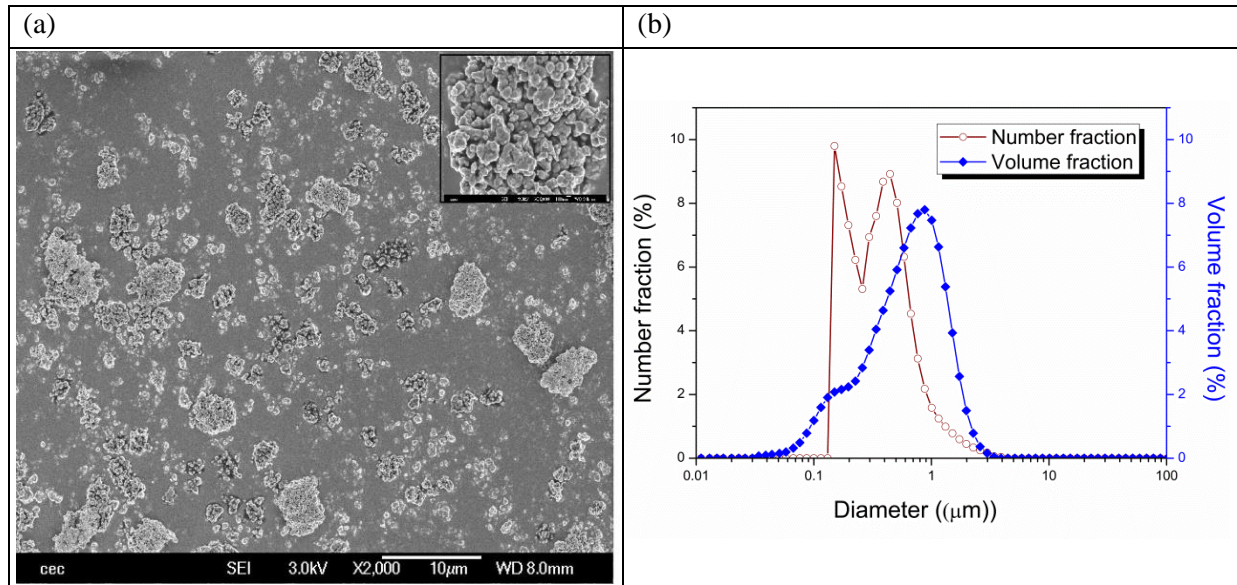
Fig. 2: Scheme of the Aerosol Deposition Device (ADM)

Fig. 3: SEM Picture (a) and particle size distribution (b) for the powder #1 (magnification 2000, white bar = 10µm: insert magnification 30000).
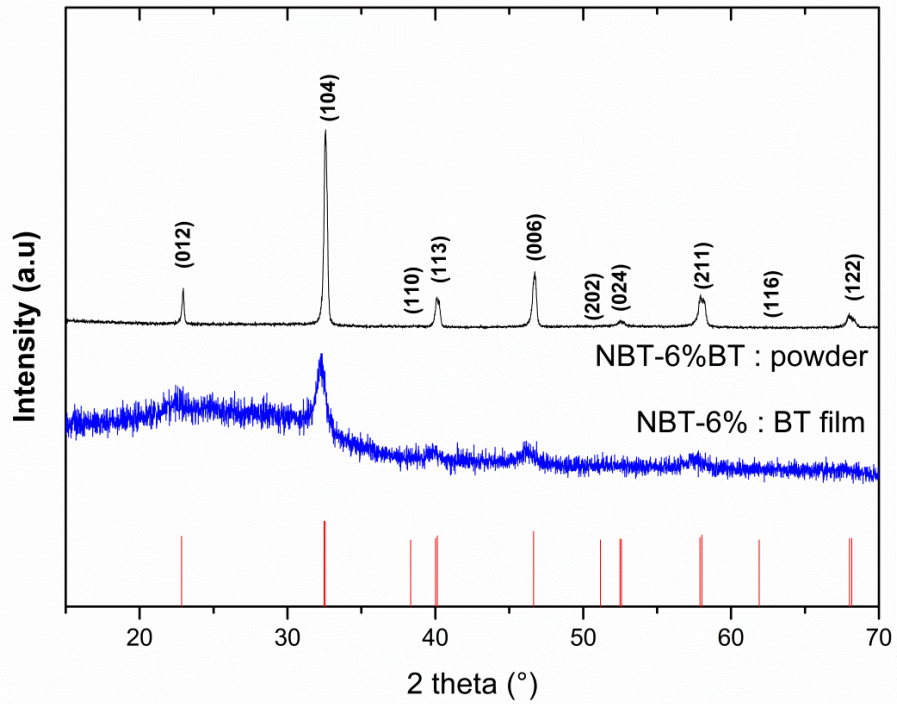
Fig. 4: X-ray diffraction pattern of powder #1 (top) and thick film #1a (bottom); The Miller index corresponds to red lines on lower part of the figure (JCPDS 012--5546 pattern of NBT-5.5% BT, indexing using hexagonal axes).
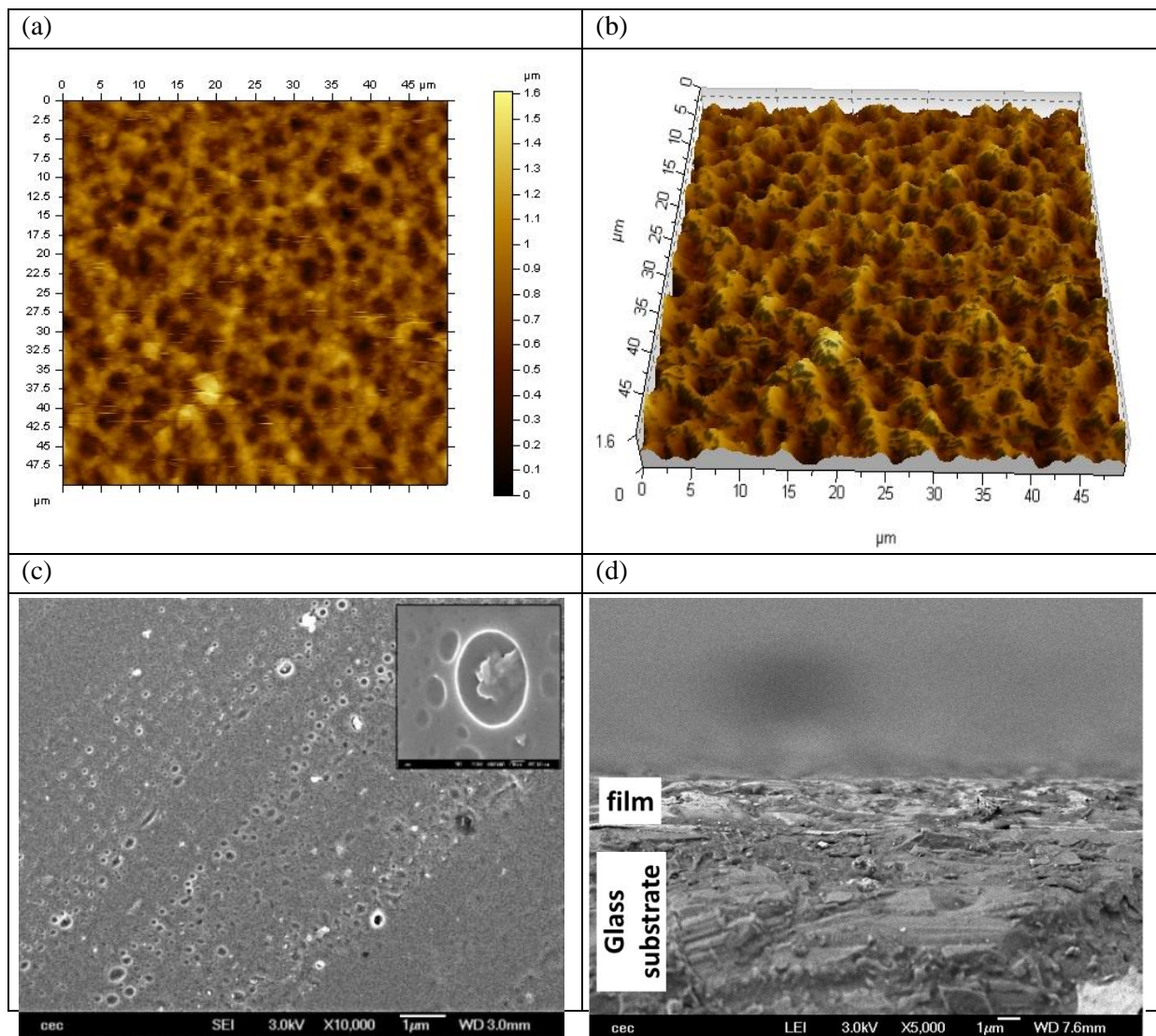
Fig. 5: (a) microstructure of sample #1a as determined by AFM for a 50µm X 50µm zone, (b) 3-D picture of the same surface), (c) SEM picture of the surface (magnification 10000, white bar = 1 µm; insert magnification 100000) and (d) SEM picture of the cross section of the sample (d) (magnification 5000, white bar = 1 µm)
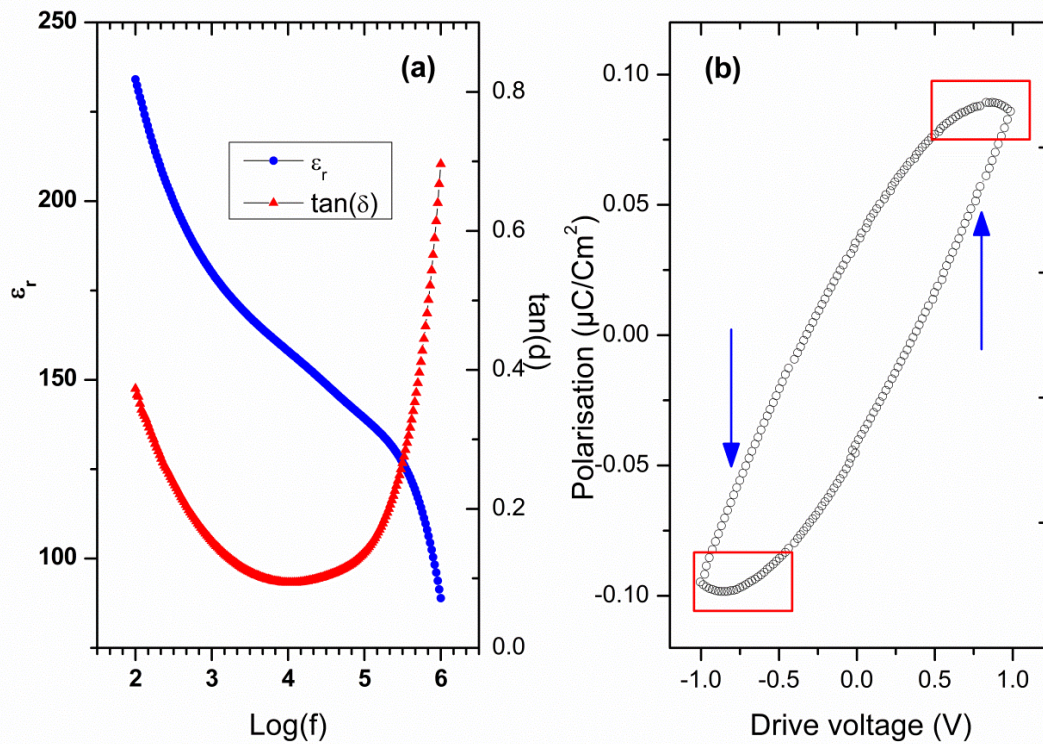
Fig 6: (a) relative permittivity and dielectric losses for sample #1b deposited on metallic substrate and (b) hysteresis cycle for the same sample (see text for blue arrows and red rectangles).